

Universality of the complete-graph Potts model with $0 < q \leq 2$

Zirui Peng,¹ Sheng Fang,^{2,3} Hao Hu,^{4,*} and Youjin Deng^{1,5,†}

¹*Department of Modern Physics, University of Science and Technology of China, Hefei, Anhui 230026, China*

²*Hefei National Research Center for Physical Sciences at the Microscales,
University of Science and Technology of China, Hefei, Anhui 230026, China*

³*School of Systems Science and Institute of Nonequilibrium Systems,
Beijing Normal University, Beijing 100875, China*

⁴*School of Physics and Optoelectronic Engineering, Anhui University, Hefei, Anhui 230601, China*

⁵*Hefei National Laboratory, University of Science and Technology of China, Hefei, Anhui 230088, China*

Universality is a fundamental concept in modern physics. For the q -state Potts model, the critical exponents are merely determined by the order-parameter symmetry S_q , spatial dimensionality and interaction range, independent of microscopic details. In a simplest and mean-field treatment—i.e., the Potts model on complete graph (CG), the phase transition is further established to be of percolation universality for the range of $0 < q < 2$. By simulating the CG Potts model in the random-cluster representation, we numerically demonstrate such a hyper-universality that the critical exponents are the same for $0 < q < 2$ and, moreover, the Ising system ($q = 2$) exhibits a variety of critical geometric properties in percolation universality. On the other hand, many other universal properties in the finite-size scaling (FSS) theory, including Binder-like ratios and distribution function of the order parameter, are observed to be q -dependent. Our finding provides valuable insights for the study of critical phenomena in finite spatial dimensions, particularly when the FSS theory is utilized.

I. INTRODUCTION

In phase transitions, such as the transition from a liquid to a gas state or from a ferromagnetic to a paramagnetic state, critical behavior describes properties of a system near its critical point. Typical critical behavior is that physical observables follow power-law functions, whose exponents characterize the scaling of the observables. Universality is a fundamental concept in understanding critical behavior. It refers to the idea that critical behavior of physical systems often depends only on a few essential characteristics, such as the spatial dimension, order-parameter symmetry and interaction range, regardless of microscopic details. Researchers usually classify phase transitions into different universality classes [1, 2], each characterized by a set of critical exponents and other universal properties. For example, many systems with short-range interactions and a scalar order parameter undergo a transition belonging to the Ising universality class [2], such as the liquid–vapor transition in simple fluids [3], the phase separation in binary fluid mixtures [4], the ferromagnetic-paramagnetic phase transition in magnetic materials, and the micellization transition in micellar systems [5]. Recent research work demonstrated the prevalence of Ising universality also in soft matter and active matter, e.g., soft-matter fluids in bulk [6], active Lennard-Jones fluids, and motility-induced phase separation in active systems [7]. Understanding universality enables us to make predictions about critical behavior of systems based on general principles, without investigating details of each system.

There exist various levels of universality for different quantities (see e.g., Ref. [8] and references therein). Critical exponents usually exhibit the strongest universality, in the sense that usually they are not affected by the specific system (on-lattice or off-lattice, percolation in site type or bond type, etc.) or boundary conditions, and only depend on the spatial dimension, the interaction range and the order-parameter symmetry. Then, there are quantities whose scaling functions also do not depend on the specific system or boundary conditions, but need metric factors for near-critical data collapsing. An example is the number of clusters per site in percolation. Besides, there exist quantities whose scaling functions are not affected by the specific system, but depend on the boundary conditions and need metric factors. Examples including the strength of the largest cluster (order parameter) and wrapping probabilities in percolation, dimensionless ratios etc. Furthermore, it is noted that statistical ensembles may renormalize the critical exponents [9] and change universal values of dimensionless quantities [10], and that the interaction anisotropy can lead to variations of universal properties [11–13].

The q -state Potts model [14] is a typical model in exploring universal critical behavior. The model is defined by the Hamiltonian $\mathcal{H} = -J \sum_{\langle ij \rangle} \delta_{\sigma_i, \sigma_j}$, where each site i possesses a spin σ_i taking one of q states (i.e., $\sigma_i = 1, 2, \dots$, or q), $\langle ij \rangle$ denotes a pair of neighboring sites, and $J > 0$ represents the ferromagnetic coupling constant. When $q = 2$, the Potts model is equivalent to the well-known Ising model. The Potts spins can be mapped to random clusters [15] through the Fortuin-Kasteleyn (FK) transformation [16, 17]. In the transformation, each bond connecting two nearest-neighboring sites with the same spin value is independently occupied with probability $p = 1 - e^{-J/kT}$, where k denotes the Boltzmann constant, T represents the temperature. The resulting

* Contact author: huhao@ahu.edu.cn

† Contact author: yjdeng@ustc.edu.cn

graph of vertices and occupied bonds corresponds to a configuration of the Potts model in the random-cluster representation. For a given graph $\mathcal{G} = (\mathcal{V}, \mathcal{E})$, with \mathcal{V} being the vertices set and \mathcal{E} being the edges (bonds) set, the Potts model in the random-cluster (RC) representation is defined by the partition function

$$Z = \sum_{A \subseteq \mathcal{E}} q^{k(A)} v^{|A|}. \quad (1)$$

Here $|A|$ is the number of occupied bonds, and $k(A)$ denotes the number of clusters (a cluster consists of vertices connected by occupied bonds; an isolated vertex is also a cluster). The bond weight is $v = p/(1-p)$, and the cluster weight is q which takes positive real numbers. When $q \rightarrow 1$, the above Potts model reduces to standard uncorrelated bond percolation [18].

The complete graph (CG) offers an accurate platform for finite-size approach to the mean-field solution. In a complete graph, there is an edge between each pair of vertices, thus each vertex interacts with all other vertices. This makes the mean-field solutions accurate on the CG. Critical exponents from the mean-field theory are quantitatively correct above the upper critical dimension, and the theory offers a qualitative picture for critical phenomena in lower dimensions. The CG Potts model has been systematically explored. For $0 < q \leq 2$, the model shows a continuous phase transition and the critical point is given by $p_c = q/V$ [19], where V is the number of vertices in the CG (also called the size of the CG). The model with $q > 2$ exhibits first-order phase transitions, and the transition point is given by $p_c = \frac{1}{V} \frac{2(q-1)}{q-2} \log(q-1)$ [14, 19].

In the limit $q \rightarrow 0$, as the above p_c corresponds to a finite $v_c/q = 1/(V-q)$, a critical configuration of the CG Potts model in the RC representation consists of a spanning forest [15, 20].

Considering universal properties of the CG Potts model with $0 < q < 2$, from theoretical results on the thermal exponent y_t and magnetic exponent y_h [19, 21], it is known that the model belongs to the universality class of standard percolation on the CG. For finite-dimensional Potts models below the upper critical dimension, critical exponents are usually continuous functions of q and the universality of the Potts model is q -dependent. For the CG Potts model with $0 < q < 2$, the above q -independence of critical exponents can be regarded as a kind of *hyper-universality*.

For $q = 2$, it has been observed that the CG Ising model in the RC representation strongly exhibits behaviors in the CG percolation universality class [22]. For example, after excluding the largest cluster, the Fisher exponent τ characterizing the critical cluster number density is consistent with $5/2$ in the percolation case. It was found that, as the size V increase, the critical configuration space has a decaying percolation sector in which clusters exhibit the CG percolation scaling behaviors. Near criticality, besides the Ising scaling window of size $O(V^{-1/2})$, the CG Ising model has a percolation scaling window of size $O(V^{-1/3})$. Outside the Ising window and in the percolation window, all clusters display the same scaling behaviors as those in critical CG percolation. Recently percolation behaviors in the CG Ising model have also been demonstrated through the loop-cluster joint model in Refs. [23, 24].

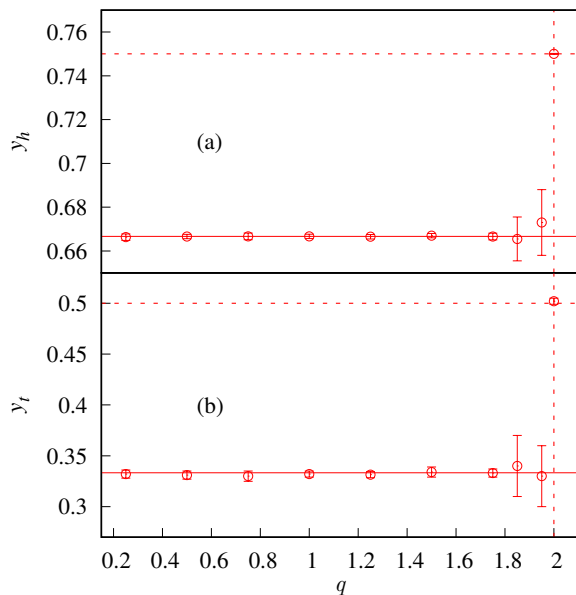


FIG. 1. Numerical estimates of critical exponents for the CG Potts model with $0 < q < 2$ are consistent with theoretical predictions of $y_h = 2/3$ and $y_t = 1/3$. With $q = 2$, the estimates are consistent with $y_h = 3/4$ and $y_t = 1/2$.

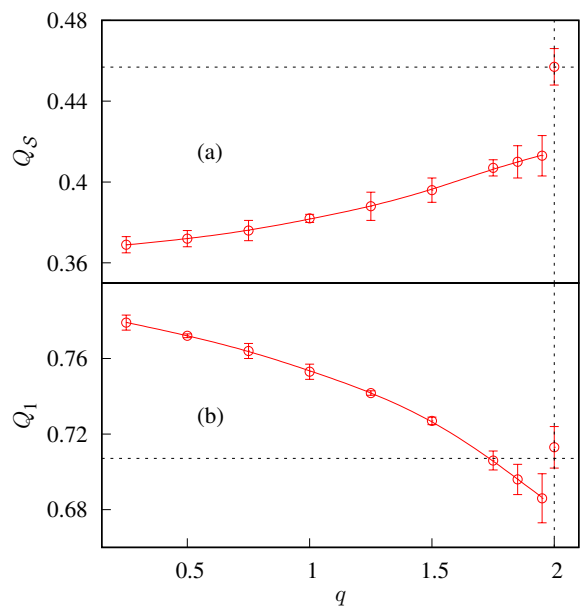


FIG. 2. The dimensionless ratios Q_S and Q_1 vary continuously for $0 < q < 2$, and show sudden changes at $q = 2$. The smooth curves are added to guide the eye.

From above results for the CG Potts model, it could be conjectured that the Fisher exponent $\tau = 5/2$ is hyper-universal in the range $0 < q \leq 2$. The hyper-universality of critical exponents appear very interesting and deserves more numerical verification. The universality of quantities besides critical exponents also deserves more investigations, e.g., it is not clear how dimensionless ratios behave as q varies. In this paper, we numerically demonstrate the hyper-universality of critical exponents and thoroughly investigate the dimensionless ratios of the CG Potts model. We have also made some improvements to the Monte Carlo algorithms for efficient simulations.

The remainder of the paper is organized as follows. Section II summarizes the main results. Section III describes the algorithms used in numerical simulations. Sections IV and V present detailed results for measured quantities, including also evidence demonstrating the efficiency of the algorithms. Section VI contains a brief conclusion and discussion.

II. MAIN RESULTS

Our main results include a demonstration of the hyper-universality of critical exponents, and the finding of q -dependence of dimensionless ratios. They are summarized as follows, while the analyses details are presented in Sections IV and V.

Firstly, for the critical exponents, our numerical results in Fig. 1 demonstrates that the magnetic renormalization exponent y_h and the thermal renormalization exponent y_t remain constant for $0 < q < 2$, i.e., they are hyper-universal. The numerical results support theoretical predictions [19, 21] of $y_h = 2/3$ and $y_t = 1/3$ for $0 < q < 2$, and of $y_h = 3/4$ and $y_t = 1/2$ for $q = 2$. Thus the model with $0 < q < 2$ are in the percolation universality class, whose critical exponents are different from the Ising universality class. Our numerical estimates for y_h come from finite-size scaling (FSS) analyses on the average of the largest-cluster size \mathcal{C}_1 , and the average of the second moment of cluster sizes $\mathcal{S}_2 = \sum_i \mathcal{C}_i^2$. To the leading order they behave as $\langle \mathcal{C}_1 \rangle \sim V^{y_h}$ and $\chi \equiv \langle \mathcal{S}_2 \rangle / V \sim V^{2y_h - 1}$. For y_t , our estimates come from FSS analyses on two covariances $\text{Cov}(\mathcal{N}_B, Q_1)$ and $\text{Cov}(\mathcal{N}_B, Q_S)$ [25–27], which both scale as $\sim V^{y_t}$ to the leading order. Here $\mathcal{N}_B = |A|$ is the number of occupied bonds in the RC representation, Q_1 and Q_S are two Binder-like dimensionless ratios defined as

$$Q_1 = \frac{\langle \mathcal{C}_1 \rangle^2}{\langle \mathcal{C}_1^2 \rangle}, \quad (2)$$

$$Q_S = \frac{\langle \mathcal{S}_2 \rangle^2}{\langle 3\mathcal{S}_2^2 - 2\mathcal{S}_4 \rangle}, \quad (3)$$

where $\mathcal{S}_4 = \sum_i \mathcal{C}_i^4$ is the fourth moment of cluster sizes. The above two covariances are correlations between \mathcal{N}_B

and the two ratios, which are defined as [25–27]

$$\begin{aligned} \text{Cov}(\mathcal{N}_B, Q_S) &= \frac{2\langle \mathcal{S}_2 \mathcal{N}_B \rangle}{\langle \mathcal{S}_2 \rangle} - \frac{\langle (3\mathcal{S}_2^2 - 2\mathcal{S}_4) \mathcal{N}_B \rangle}{\langle 3\mathcal{S}_2^2 - 2\mathcal{S}_4 \rangle} - \langle \mathcal{N}_B \rangle, \\ \text{Cov}(\mathcal{N}_B, Q_1) &= \frac{2\langle \mathcal{C}_1 \mathcal{N}_B \rangle}{\langle \mathcal{C}_1 \rangle} - \frac{\langle \mathcal{C}_1^2 \mathcal{N}_B \rangle}{\langle \mathcal{C}_1^2 \rangle} - \langle \mathcal{N}_B \rangle. \end{aligned} \quad (4)$$

We have also analyzed the Fisher exponent τ and the two-arm exponent x_2 , as defined in Sections IV B and IV C, respectively. The exponent τ is associated with the cluster number density and our numerical results show that τ is invariant for $0 < q \leq 2$, supporting the conjecture of the hyper-universality of τ in the Introduction. Our analyses suggest that the two-arm exponent x_2 is related to the number of vertices visited in the simultaneous breadth-first searches of the Sweeny Monte Carlo algorithm, i.e., the latter number scale as $V^{y_h - x_2} \sim \log V$ for $0 < q < 2$, where y_h takes the percolation value $2/3$. This indicates $x_2 = 2/3$ for $0 < q < 2$, demonstrating the hyper-universality of x_2 . The above scaling also explains the high efficiency of the Sweeny algorithm.

Secondly, in contrast to the above q -independent critical exponents, as shown in Fig. 2, we find that dimensionless ratios Q_S and Q_1 continuously change for $0 < q < 2$ and exhibit jumps at $q = 2$. These tell that, as in other models, the dimensionless ratios are less universal than critical exponents in the CG Potts model. The sudden changes at $q = 2$ is related to the fact that the CG Potts model with $0 < q < 2$ and the model with $q = 2$ belong to different universality classes (as categorized by values of critical exponents y_t and y_h). The q -dependence of dimensionless ratios reflects the variation of universal scaling functions of cluster-size distributions, which is carefully observed in Sec. V.

III. ALGORITHMS

Markov Chain Monte Carlo (MCMC) algorithms have proven to be effective tools for simulating the Potts model. Two widely used MCMC algorithms are the Swendsen-Wang-Chayes-Machta (SWCM) algorithm [28, 29] and the Sweeny [30] algorithm. The SWCM algorithm utilizes non-local cluster updates and exhibits high efficiency for Potts model with $q > 1$. For the Potts

Algorithm 1: Swendsen-Wang-Chayes-Machta algorithm for the CG Potts model

- 1 Independently for each cluster i ($= 1, \dots, k(A)$),
generate a random number $P_i \in [0, 1)$
 - 2 **if** $P_i \leq 1/q$ **then**
 - 3 | The cluster is classified as “active”
 - 4 **else**
 - 5 | The cluster is classified as “inactive”
 - 6 **end**
 - 7 Update all “active” clusters as the bond percolation.
 - 8 Update the information of all clusters.
-

model with $0 < q < 1$, the Sweeny algorithm is the only known MCMC algorithm and it shows rich dynamic behaviors [31]. For bond percolation ($q = 1$), a configuration can be easily generated by independently occupying each edge with the same probability.

The SWCM algorithm for CG Potts model is presented in Alg. 1. It mainly involves two steps: for a given bond configuration independently deem each cluster to be “active” with probability $1/q$ and “inactive” otherwise; then update all “active” clusters as uncorrelated bond percolation with occupation probability $p = v/(v+1)$. Hereafter this work focuses on the critical point of the CG Potts model with $0 < q \leq 2$, thus bond percolation in the latter step has $p = p_c = q/V$. It is noted that this p_c is different from bond percolation threshold $1/V'$, where V' is the number of vertices in all “active” clusters.

For percolation in the SWCM algorithm, the bond occupation probability $p = q/V$ is rather small for large V . This implies that many operations would be needed if all candidate bonds were visited to decide whether or not they are occupied. One can use a more efficient procedure as in Refs. [32–34], which is described as follows. Considering i candidates bonds, we define $P(i) \equiv (1-p)^{i-1}p$ to be the probability that the first $(i-1)$ bonds are unoccupied while the i th bond is occupied. The cumulative probability is calculated as $F(i) = \sum_{j=1}^i P(j) = 1 - (1-p)^i$, which gives the probability that the first occupied bond has its index less than or equal to i . After occupying one bond i_0 , one gets the next occupied bond $(i_0 + i)$ by drawing a uniformly distributed random number $0 \leq r < 1$. The value of i satisfies

$$F(i-1) \leq r < F(i). \quad (5)$$

From the above equation one derives

$$i = 1 + \lceil \log(r)/\log(1-p_c) \rceil. \quad (6)$$

Algorithm 2: Modified Sweeny algorithm for the CG Potts model

- 1 Choose an operation randomly — adding a bond or deleting a bond
 - 2 **if** *Adding a bond* **then**
 - 3 Choose an empty bond xy uniformly at random
 - 4 **if** xy connected via a path not including xy **then**
 - 5 Occupy xy with probability $\min\{1, P_{BB}^{(+)}\}$
 - 6 **else**
 - 7 Occupy xy with probability $\min\{1, P_{BR}^{(+)}\}$
 - 8 **end**
 - 9 **else if** *Deleting a bond* **then**
 - 10 Choose an occupied bond xy uniformly at random
 - 11 **if** xy connected via a path not including xy **then**
 - 12 Delete xy with probability $\min\{1, P_{BB}^{(-)}\}$
 - 13 **else**
 - 14 Delete xy with probability $\min\{1, P_{BR}^{(-)}\}$
 - 15 **end**
 - 16 **end**
-

The above process is iterated until the status of all candidate bonds are determined. The procedure is efficient as one jumps between occupied bonds, without explicitly considering the occupation of all candidate bonds one by one. This approach significantly enhances the simulation efficiency for models with small p . It is particularly advantageous for the CG model which has a large total number of bonds.

For the Sweeny algorithm, a basic step is proposing to change the status of a randomly selected bond, then accepting the proposal according to the Metropolis-Hastings criterion [35, 36]. More precisely, if xy is an empty bond, it will be occupied with probability $\min\{1, v\}$ (resp. $\min\{1, v/q\}$) in case that two endpoints x and y are (resp. are not) connected via a path not including xy . If xy is an occupied bond, it will be erased with probability $\min\{1, 1/v\}$ (resp. $\min\{1, q/v\}$), in case that two endpoints of xy are (resp. are not) connected via a path not including xy . For this original Sweeny algorithm, a problem arises when V becomes large: at $v = v_c = q/(V-q)$, probabilities of updates occupying an empty bond are proportional to $q/(V-q)$ or $1/(V-q)$, which become very small for large V . This would cause a severely slowing-down of the simulations [31]. Similar to our previous work [31], we propose a modified Sweeny algorithm for CG Potts model, as depicted in Alg. 2.

In the original Sweeny algorithm, the probability of proposing the occupation of an empty bond is high, but the corresponding acceptance probabilities are low. In the modified algorithm, we increase the acceptance probabilities by equalizing proposal probabilities of adding and deleting bonds. The acceptance probabilities in Alg. 2 are derived as follows. Using A and B to represent two configurations that can transform into each other in an update, the detailed balance condition has the form

$$\begin{aligned} & \pi(A)P_{\text{pro}}(A \rightarrow B)P_{\text{acc}}(A \rightarrow B) \\ & = \pi(B)P_{\text{pro}}(B \rightarrow A)P_{\text{acc}}(B \rightarrow A), \end{aligned} \quad (7)$$

where π is the configuration weight, P_{pro} and P_{acc} are the proposal and acceptance probabilities, respectively. The detailed balance condition associated with the addition or deletion of a bond can be written as

$$\begin{aligned} & \frac{1}{\mathcal{N}_B - \mathcal{N}_B(A)} \times q^{k(A)} v^{\mathcal{N}_B(A)} \times P_{\text{acc}}(A \rightarrow B) \\ & = \frac{1}{\mathcal{N}_B(B)} \times q^{k(B)} v^{\mathcal{N}_B(B)} \times P_{\text{acc}}(B \rightarrow A). \end{aligned} \quad (8)$$

Considering the case where $A \rightarrow B$ represents the occupation of a bond xy ($B \rightarrow A$ represents the deletion of the bond): when x and y are (resp. not) connected through a path that does not include the bond xy , one observes that $k(A) = k(B)$ (resp. $k(A) - 1 = k(B)$) and $\mathcal{N}_B(A) + 1 = \mathcal{N}_B(B)$. Following the Metropolis-Hastings

criterion, at $v = v_c$ the acceptance probabilities in Alg. 2 are calculated as

$$P_{BB}^{(+)} = \min\left\{1, \frac{\mathcal{N} - \mathcal{N}_B}{\mathcal{N}_B + 1} \times \frac{q}{V - q}\right\}, \quad (9)$$

$$P_{BR}^{(+)} = \min\left\{1, \frac{\mathcal{N} - \mathcal{N}_B}{\mathcal{N}_B + 1} \times \frac{1}{V - q}\right\}, \quad (10)$$

$$P_{BB}^{(-)} = \min\left\{1, \frac{\mathcal{N}_B}{\mathcal{N} - \mathcal{N}_B + 1} \times \frac{V - q}{q}\right\}, \quad (11)$$

$$P_{BR}^{(-)} = \min\left\{1, \frac{\mathcal{N}_B}{\mathcal{N} - \mathcal{N}_B + 1} \times \frac{V - q}{1}\right\}. \quad (12)$$

Given $\mathcal{N} = \frac{V(V-1)}{2}$ and $\langle \mathcal{N}_B \rangle \simeq \frac{V}{2}$ [19], for large V we estimate that

$$P_{BB}^{(+)} \simeq \min\{1, q\}, \quad (13)$$

$$P_{BR}^{(+)} \simeq 1, \quad (14)$$

$$P_{BB}^{(-)} \simeq \min\left\{1, \frac{1}{q}\right\}, \quad (15)$$

$$P_{BR}^{(-)} \simeq 1. \quad (16)$$

Thus, the acceptance probabilities in our revised algorithm does not decrease when V becomes large.

We note that a primary challenge of the Sweeney algorithm lies in verifying the connectivity between two endpoints of a chosen bond. For two-dimensional lattices, there are three common algorithms with distinct different asymptotic running-time properties: breadth-first search, union-find, and dynamic-connectivity algorithms [37, 38]. For the CG Potts model, we use the method of simultaneous breadth-first searches starting at both end points of a bond xy , which is efficient as analyzed in Sec. IV C.

IV. HYPER-UNIVERSALITY OF CRITICAL EXPONENTS

In this section, we demonstrate the hyper-universality of critical exponents for the CG Potts model. It is numerically verified that the renormalization exponents y_t , y_h , the exponent τ describing the cluster number density, and the two-arm exponent x_2 all keep invariant in the range $0 < q < 2$, and that the invariance of τ extends to $q = 2$. When $0 < q < 2$, we also show that $x_2 = y_h$ explains the efficiency of using simultaneous breath-first searches in the Sweeny algorithm.

A. Renormalization exponents y_t and y_h

The exponents y_t and y_h have been theoretically derived for the CG Potts model with $0 < q \leq 2$. The model was first systematically studied in Ref. [19], and then extended to a broad family of pseudo-critical points in Ref. [21]. Defining $\varepsilon \equiv |p - p_c|/p_c$ with $p_c = q/V$, these works derived the following:

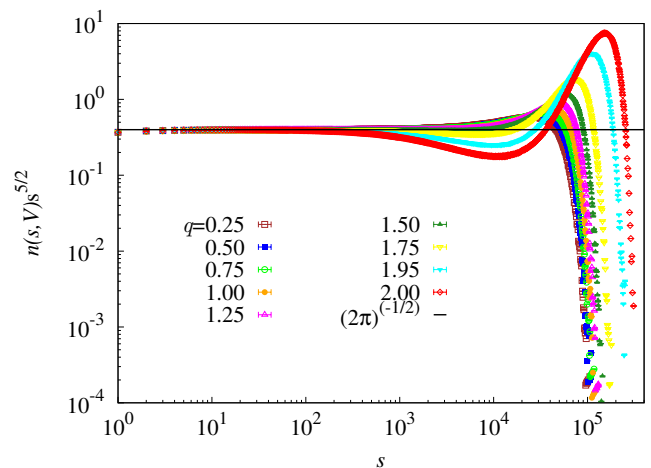


FIG. 3. The scaled cluster number density $n(s, V)s^{5/2}$ versus the cluster size s for the CG Potts model with different q . The data were obtained from simulations at fixed $V = 2^{22}$. The horizontal straight line represents a theoretical prediction of $n(s, V)s^{5/2} = (2\pi)^{-1/2}$ for small s [39].

- (i) For $0 < q < 2$, when $p = \frac{q}{V}(1 \pm \varepsilon)$ with $\varepsilon \leq O(V^{-1/3})$, the largest cluster scales as $\langle \mathcal{C}_1 \rangle \sim V^{2/3}$;
- (ii) For $q = 2$, when $p = \frac{2}{V}(1 \pm \varepsilon)$ with $\varepsilon \leq O(V^{-1/2})$, the largest cluster behaves as $\langle \mathcal{C}_1 \rangle \sim V^{3/4}$.

From finite-size scaling theory, usually the size of a critical scaling window scales as $O(V^{-y_t})$, and the largest cluster behaves as $\langle \mathcal{C}_1 \rangle \sim V^{y_h}$. Thus, when $0 < q < 2$, from (i), the CG Potts model belongs to the percolation universality class with $y_t = 1/3$ and $y_h = 2/3$; when $q = 2$, from (ii), the model falls within the Ising universality class with $y_t = 1/2$ and $y_h = 3/4$. To demonstrate the theoretical results, we numerically determined y_h and y_t as plotted in Fig. 1. Simulations were performed for different sizes V at the critical point. Then the data were fitted to the formula $aV^{y_0}(1 + b_1V^{y_1}) + c_0$ using the least-square method, where $y_0 > 0$ is the leading scaling exponent and $y_1 < 0$ is the leading correction exponent. Estimates of y_h come from fitting results of $\langle \mathcal{C}_1 \rangle$ and $\langle \mathcal{S}_2 \rangle / V$, for which $y_0 = y_h$ and $2y_h - 1$, respectively. Estimates of y_t come from fitting the data of covariances $\text{Cov}(\mathcal{N}_B, Q_1)$ and $\text{Cov}(\mathcal{N}_B, Q_S)$, for which $y_0 = y_t$. Figure 1 shows that our numerical results of y_t and y_h are consistent with theoretical predictions in last paragraph, thus supporting the hyper-universality of y_t and y_h for the CG Potts model with $0 < q < 2$.

B. Critical exponent τ

The exponent τ describes the cluster number density $n(s, V)$. The quantity $n(s, V)\Delta s$ gives the number of clusters with sizes in $[s, s + \Delta s]$, normalized by the system size V . For standard percolation ($q = 1$) on the CG,

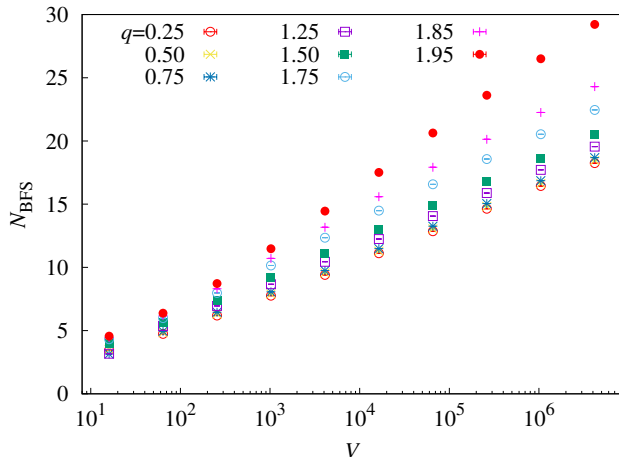


FIG. 4. Numerical results of the number of vertices N_{BFS} that are needed to be searched in the simultaneous breadth-first searches of the Sweeny algorithm. The approximate linearity in the semi-log plot suggests that $N_{\text{BFS}} \sim \log V$ for $0 < q < 2$.

Ref. [39] predicts that $n(s, V)$ follows a standard scaling form

$$n(s, V) = n_0 s^{-\tau} \tilde{n}(s/V^{d_f}) \quad [\tilde{n}(x \rightarrow 0) = 1], \quad (17)$$

with $n_0 = (2\pi)^{-1/2}$, $d_f = y_h = 2/3$, and $\tau = 5/2$. For the CG Potts model with $q = 2$, in Ref. [22] it was observed that τ and n_0 have the same value as the $q = 1$ model, though exponents y_t and y_h are different for the $q = 2$ and $q = 1$ models. For these results, we conjecture that for other models with $q \in (0, 2]$, values of n_0 and τ also have the same values as the $q = 1$ model. We plotted our numerical results of $n(s, V)$ in Fig. 3. The figure shows that, for small values of s , $n(s, V)s^{5/2}$ is consistent with $(2\pi)^{-1/2}$, which demonstrates the above conjecture. The deviations at large s are supposed to be accounted by finite-size effects. Thus, the critical exponent τ is hyper-universal for $0 < q \leq 2$.

Results on the CG Ising model ($q = 2$) can be understood by the loop-cluster (LC) joint model [23]. For the CG Ising model in the loop representation, the bond density decays as $V^{-1/2}$, which means that the loop configurations are almost vacant in the thermodynamic limit [24]. Under the LC joint model, a LC algorithm passes back and forth between the loop and FK cluster representations. The process from the loop to the FK configuration is like a conventional percolation process [24]. During this process, almost all loops are connected together to form the largest FK cluster, and other FK clusters are basically standard percolation clusters. In other words, for the CG Ising model, only the largest cluster demonstrates the Ising property, while other clusters manifest percolation properties. These observations underscore the profound intricacy and richness of universality.

C. Two-arm exponent x_2

On a finite-dimensional lattice, the k -arm exponent x_k describes the probability that k neighboring vertices within $O(1)$ distances connect to the surface of a (hyper-) sphere of radius R through k distinct clusters, i.e., for large R the probability asymptotically scales as $p_k(R) \sim R^{-x_k}$. For a finite-size lattice of linear size L , at criticality one has $p_k(L) \sim L^{-x_k}$. When employing the Sweeny algorithm, we use the method of simultaneous breadth-first searches [37, 40], which start at both endpoints of a bond xy to check if x and y are connected via a path not including xy . This method of simultaneous searches has very simple code and is effective enough for small and medium lattice sizes, as demonstrated in Ref. [40]. When x and y are not connected via a path not including xy , the two endpoints are associated with two distinct clusters if assuming the bond xy is unoccupied, and Ref. [40] shows that the average size of the smaller cluster scales as $\sim L^{d_F - x_2}$ on the square lattice, where d_F is the fractal dimension and x_2 is the two-arm exponent [41].

For the CG of size V , though the Euclidean distance cannot be defined, one can similarly define $p_k(V)$ as the probability that there exist k pairs of vertices, where two vertices in a pair belong to a same cluster and different pairs are in distinct clusters. At criticality, similarly we define that the k -arm exponent x_k describes the probability as $p_k(V) \sim V^{-x_k}$. For $k = 1$, considering that sizes of critical clusters scale as V^{d_f} (which is true for $0 < q < 2$), with $d_f = y_h$ being the volume fractal dimension, the probability of two vertices being in the same cluster is given by $p_1(V) \sim V^{y_h - 1}$, i.e., $x_1 = 1 - y_h$. In the limit of $V \rightarrow \infty$ on the CG, it is expected that selections of k pairs of vertices become mutually independent, which indicates $x_k = k(1 - y_h)$.

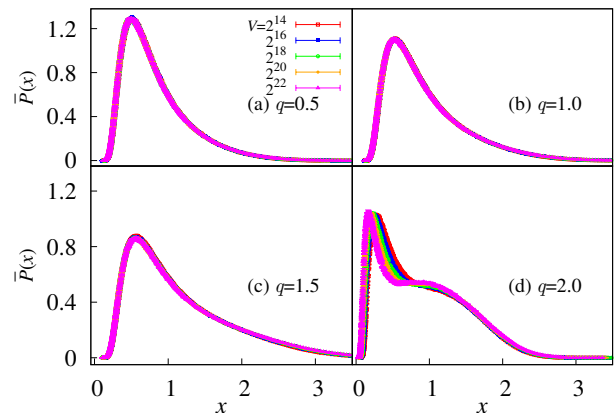


FIG. 5. The probability distribution function $\bar{P}(x)$ versus x at (a) $q = 0.5$, (b) $q = 1$, (c) $q = 1.5$ and (d) $q = 2$. The variable $x \equiv \mathcal{C}_1 / \langle \mathcal{C}_1 \rangle$, where $\langle \mathcal{C}_1 \rangle \sim V^{y_h}$ with $y_h = 2/3$ for $0 < q < 2$ and $y_h = 3/4$ for $q = 2$.

Similar to that on finite-dimensional lattices, on the CG we assume that the number of vertices N_{BFS} needed to be searched in the simultaneous breadth-first searches of the Sweeny algorithm scales as $\sim V^{y_h - x_2}$. We measured N_{BFS} to determine x_2 . From Fig. 4, it is seen that $N_{\text{BFS}} \sim \log V$ for $0 < q < 2$ (for $q = 1$, the Sweeny algorithm is not needed and we did not measure N_{BFS}). The logarithmic behavior suggest that the Sweeny algorithm with simultaneous breadth-first searches is a very efficient method for simulating the CG Potts model. The logarithmic behavior also indicates $x_2 = y_h$ for $0 < q < 2$. Thus, for $0 < q < 2$, one has $x_2 = y_h = 2/3$, i.e., it is hyper-universal.

V. q -DEPENDENT DIMENSIONLESS RATIOS AND THE CLUSTER-SIZE DISTRIBUTIONS

While critical exponents are found to be hyper-universal, we find that critical dimensionless ratios still depend on the parameter q , as demonstrated for the ratios Q_S and Q_1 in Fig. 2. In this section, we present details for estimating the dimensionless ratios. We also attribute the variation of the ratios to the change of the cluster-size distributions.

To estimate critical values of dimensionless ratios, the data were fitted to the formula $Q(V) = Q_0 + b_1 V^{y_1} + b_2 V^{y_2}$ using the least-square method, where Q_0 represents the value of a ratio Q in the thermodynamic limit $V \rightarrow \infty$, $y_2 < y_1 < 0$ are correction exponents, b_1 and b_2 are non-universal amplitudes. Several fits with different values of y_1 and y_2 were performed to provide a reliable estimate. For example, the fitting details for Q_1 at $q = 2$ are provided in Table I. Estimated values of Q_S and Q_1 for $0 < q \leq 2$ are summarized in Table II and plotted in Fig. 2. For $q = 2$, the numerical estimates are consistent

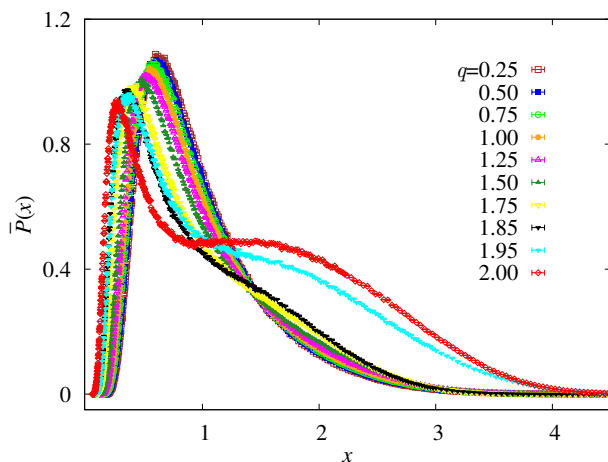


FIG. 6. The probability distribution function $\bar{P}(x)$ versus x at $V = 2^{22}$. The variable $x \equiv \mathcal{C}_1 / \langle \mathcal{C}_1 \rangle$, where $\langle \mathcal{C}_1 \rangle \sim V^{y_h}$ with $y_h = 2/3$ for $0 < q < 2$ and $y_h = 3/4$ for $q = 2$. The function $\bar{P}(x)$ evolves as q changes.

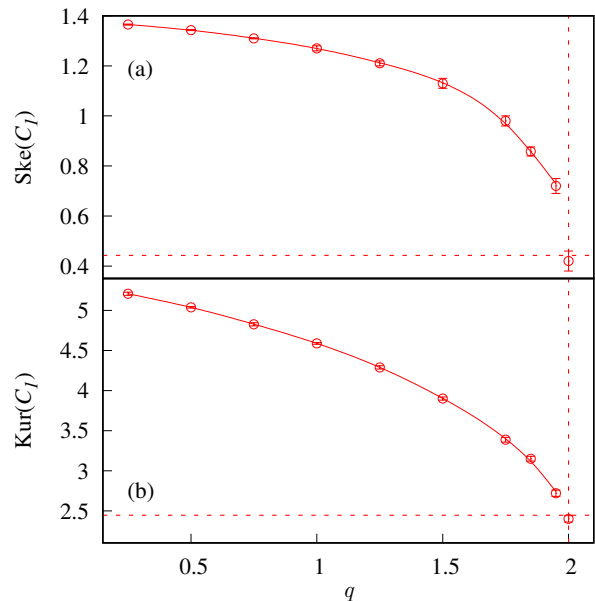


FIG. 7. The skewness $\text{Ske}(\mathcal{C}_1)$ and kurtosis $\text{Kur}(\mathcal{C}_1)$ versus q . The smooth curves are added to guide the eye, and they are not drawn to $q = 2$ due to a possible discontinuity.

with theoretical values derived in the Appendix.

From Table II and Fig. 2, it is seen that both Q_S and Q_1 change continuously for $0 < q < 2$, and they display jumps at $q = 2$. As presented in Sec. IV A, the largest cluster is govern by $y_h = 3/4$ at $q = 2$, in contrast to $y_h = 2/3$ for $0 < q < 2$. This difference should be related to the jumps of the ratios at $q = 2$. For $0 < q < 2$, the continuous variation of the ratios originates from changes of the cluster-size distributions. To illustrate the latter point, we first define $P(\mathcal{C}_1, V)d\mathcal{C}_1$ as the probability that the largest cluster has its size between \mathcal{C}_1 and $\mathcal{C}_1 + d\mathcal{C}_1$, then calculate the probability distribution function $\bar{P}(x)dx$ with $x \equiv \mathcal{C}_1 / \langle \mathcal{C}_1 \rangle$. The function $\bar{P}(x)$ is depicted in Fig. 5 for several q values. At fixed q , the functions asymptotically overlap at large sizes V , reflecting a kind of universality. However, when comparing the functions at different q values, as plotted in Fig. 6, one sees that $\bar{P}(x)$ is not universal for different q . This explains the q -dependent behavior of Q_1 , which characterizes the relative fluctuation of \mathcal{C}_1 .

Besides the fluctuation, we also measured the skewness $\text{Ske}(\mathcal{C}_1)$ and kurtosis $\text{Kur}(\mathcal{C}_1)$ of the distribution of \mathcal{C}_1 , defined as

$$\text{Ske}(\mathcal{C}_1) = \mu_3 / \mu_2^{3/2}, \quad (18)$$

$$\text{Kur}(\mathcal{C}_1) = \mu_4 / \mu_2^2, \quad (19)$$

where $\mu_i(\mathcal{C}_1) = \langle (\mathcal{C}_1 - \langle \mathcal{C}_1 \rangle)^i \rangle$. The skewness quantifies the asymmetry of the probability distribution of a random variable relative to its mean, while the kurtosis measures the “tailedness” of the distribution. Results for $\text{Ske}(\mathcal{C}_1)$ and $\text{Kur}(\mathcal{C}_1)$ are summarized in Table II and

TABLE I. Fit results for Q_1 at $q = 2$. The simulation data were fitted to the formula $Q_1(V) = Q_{1,0} + b_1V^{y_1} + b_2V^{y_2}$ using the least-square method. Only data with $V \geq V_{\min}$ were included in the fits to eliminate effects from higher-order corrections. “DF” is short for degrees of freedom in the fits.

V_{\min}	$Q_{1,0}$	y_1	y_2	b_1	b_2	χ^2/DF
2^8	0.708(4)	-0.124(9)	$2y_1$	-0.06(3)	0.36(2)	3.2/4
2^{10}	0.713(10)	-0.111(19)	$2y_1$	-0.10(7)	0.37(3)	2.76/3
2^8	0.707(3)	-0.16(1)	$3/2y_1$	-0.14(6)	0.43(4)	3.22/4
2^{10}	0.712(9)	-0.14(3)	$3/2y_1$	-0.2(1)	0.47(8)	2.74/3
2^{10}	0.706(4)	-1/6	-1/4	-0.10(1)	0.43(2)	5.63/5
2^{12}	0.707(2)	-1/6	-1/4	-0.13(2)	0.45(4)	3.87/3

TABLE II. Estimates of Q_S , Q_1 , $\text{Ske}(\mathcal{C}_1)$ and $\text{Kur}(\mathcal{C}_1)$. The last column contains theoretical predictions at $q = 2$ derived in the Appendix.

q	0.25	0.5	0.75	1	1.25	1.5	1.75	1.85	1.95	2	2 (theo.)
Q_S	0.369(4)	0.372(4)	0.3761(5)	0.382(2)	0.388(7)	0.396(6)	0.407(4)	0.410(8)	0.413(10)	0.457(9)	0.4569
Q_1	0.779(3)	0.772(2)	0.764(4)	0.753(4)	0.7417(12)	0.727(2)	0.706(5)	0.696(8)	0.686(13)	0.713(11)	0.7071
$\text{Ske}(\mathcal{C}_1)$	1.365(2)	1.343(2)	1.310(2)	1.27(1)	1.21(1)	1.128(21)	0.984(24)	0.858(18)	0.715(30)	0.417(40)	0.4428
$\text{Kur}(\mathcal{C}_1)$	5.21(2)	5.04(1)	4.83(2)	4.59(1)	4.29(2)	3.90(2)	3.39(3)	3.15(3)	2.72(4)	2.40(4)	2.4446

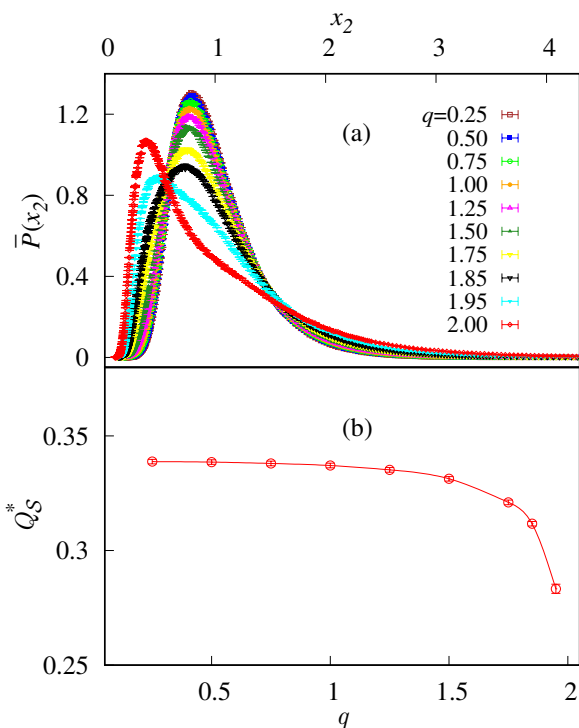


FIG. 8. (a) The probability distribution function $\bar{P}(x_2)$ associated with the second-largest cluster at $V = 2^{22}$. Here the variable $x_2 \equiv \mathcal{C}_2/\langle \mathcal{C}_2 \rangle$, where $\langle \mathcal{C}_2 \rangle \sim V^{2/3}$ for $0 < q < 2$ and $\sim V^{1/2} \log V$ for $q = 2$ [22]. (b) The dimensionless ratio Q_S^* versus q . The smooth curve is added to guide the eye. For $q = 2$, a reliable numerical estimate of Q_S^* is not available due to large finite-size corrections.

plotted in Fig. 7. It is seen that both quantities decrease with increasing q . At $q = 2$, from results on Q_1 , it could be expected that $\text{Ske}(\mathcal{C}_1)$ and $\text{Kur}(\mathcal{C}_1)$ also change discontinuously. Comparing Fig. 2(b) and Fig. 7, the

discontinuity would be much smaller for the latter two quantities if it were there.

Finally, we ask that, after excluding the largest cluster, whether one could still observe significant change of the size distributions as q varies. We observed the size of the second-largest cluster \mathcal{C}_2 , and a modified dimensionless ratio Q_S^* defined as

$$Q_S^* = \frac{\langle \mathcal{S}_2^* \rangle^2}{\langle 3\mathcal{S}_2^{*2} - 2\mathcal{S}_4^* \rangle}, \quad (20)$$

where the modified moments are $\mathcal{S}_k^* = \mathcal{S}_k - \mathcal{C}_1^k$. As plotted in Fig. 8(a), we find that the distribution of \mathcal{C}_2 varies significantly as q changes. From Fig. 8(b), one sees that the ratio Q_S^* decreases with increasing q , while Q_S being monotonically increasing with q in Fig. 2. Thus, excluding the largest cluster does not eliminate the q -dependent variation of the size distributions, though it causes their obvious changes.

VI. CONCLUSION AND DISCUSSION

In summary, by MCMC simulations and FSS analyses, we have studied universal properties of the CG Potts model with $0 < q \leq 2$. The critical exponents are numerically demonstrated to be hyper-universal, e.g., exponents y_t , y_h and x_2 are invariant for $0 < q < 2$, τ is invariant for $0 < q \leq 2$. However, q -dependent variations are still observed in Binder-like dimensionless ratios, which are attributed to changes of the distribution functions of the cluster sizes. In simulations, we have implemented an improved Sweeny algorithm, and verified the high efficiency of using simultaneous breadth-first searches in the algorithm.

The above results on the CG represent mean-field behaviors of the Potts model. We suppose that the behaviors could also be observed for the Potts model with

$0 < q \leq 2$ above the upper critical dimension. The percolation model has its upper critical dimension as $d_c = 6$ [42], and the Ising model has two upper critical dimensions $d_c = 4$ and 6 [43]. Simulations of the Potts model above d_c are needed to check if similar behaviors indeed present. For these simulations above d_c , the improved Sweeny algorithm with simultaneous breadth-first searches is also expected to be highly efficient. To analyze results above d_c , unlike for the models on the CG, the influence of boundary conditions could be vital in the FSS [44–46].

ACKNOWLEDGMENTS

This work was supported by the National Natural Science Foundation of China under Grants No. 12275263 (Y.D.) and No. 12375026 (H.H.), the Innovation Program for Quantum Science and Technology under Grant No. 2021ZD0301900, and the Natural Science Foundation of Fujian Province of China under Grant No. 2023J02032.

Appendix: Theoretical calculations of Binder-like ratios at $q = 2$.

In this appendix we give the theoretical predictions of Q_S , Q_1 , $\text{Ske}(\mathcal{C}_1)$ and $\text{Kur}(\mathcal{C}_1)$ for $q = 2$. The last three quantities can be derived from the probability distribution $P(\mathcal{C}_1, V)$. For this purpose we reformulate the distribution function by using $\tilde{P}(\tilde{x})d\tilde{x} = P(\mathcal{C}_1, V)d\mathcal{C}_1$, where $\tilde{x} \equiv \mathcal{C}_1/V^{d_f}$ with $d_f = y_h = 3/4$ at $q = 2$. Following Eq. (32) in Ref. [21] and Eq. (3) in Ref. [22], as $V \rightarrow \infty$ the limiting distribution function is

$$\tilde{P}(\tilde{x}) = \frac{\exp(-\tilde{x}^4/12)}{\int_0^\infty \exp(-t^4/12)dt}. \quad (\text{A.1})$$

The k th moment $\langle \mathcal{C}_1^k \rangle$ is

$$\langle \mathcal{C}_1^k \rangle = V^{3k/4} \frac{\int_0^\infty \tilde{x}^k \exp(-\tilde{x}^4/12)d\tilde{x}}{\int_0^\infty \exp(-t^4/12)dt}. \quad (\text{A.2})$$

Then the Binder-like ratios can be calculated as

$$Q_1 = \frac{\langle \mathcal{C}_1 \rangle^2}{\langle \mathcal{C}_1^2 \rangle} \simeq 0.707107, \quad (\text{A.3})$$

$$\text{Ske}(\mathcal{C}_1) = \frac{\langle \mathcal{C}_1^3 \rangle - 3\langle \mathcal{C}_1^2 \rangle \langle \mathcal{C}_1 \rangle + 2\langle \mathcal{C}_1 \rangle^3}{(\langle \mathcal{C}_1^2 \rangle - \langle \mathcal{C}_1 \rangle^2)^{3/2}} \simeq 0.442787, \quad (\text{A.4})$$

$$\text{Kur}(\mathcal{C}_1) = \frac{\langle \mathcal{C}_1^4 \rangle - 4\langle \mathcal{C}_1^3 \rangle \langle \mathcal{C}_1 \rangle + 6\langle \mathcal{C}_1^2 \rangle \langle \mathcal{C}_1 \rangle^2 - 3\langle \mathcal{C}_1 \rangle^4}{(\langle \mathcal{C}_1^2 \rangle - \langle \mathcal{C}_1 \rangle^2)^2} \simeq 2.44465. \quad (\text{A.5})$$

As for the Q_S , for the CG Potts model with $q = 2$, one has $Q_S = Q_m$, where $Q_m \equiv \langle m^2 \rangle^2 / \langle m^4 \rangle$ is the Binder-like ratio for the magnetization m . From Eq.(A.14) in Ref. [47], one gets

$$Q_m = 4 \left[\frac{\Gamma(\frac{3}{4})}{\Gamma(\frac{1}{4})} \right]^2 + \frac{16}{5} \sqrt{3} \left[\frac{\Gamma(\frac{3}{4})}{\Gamma(\frac{1}{4})} \right]^3 \frac{1}{\sqrt{V}} + \mathcal{O}\left(\frac{1}{V}\right) \simeq 0.456947 + 0.214002 \frac{1}{\sqrt{V}} + \mathcal{O}\left(\frac{1}{V}\right). \quad (\text{A.6})$$

Thus we have $Q_S = Q_m \simeq 0.456947$ in the limit $V \rightarrow \infty$.

-
- [1] K. G. Wilson, Rev. Mod. Phys. **55**, 583 (1983).
 - [2] A. Pelissetto and E. Vicari, Phys. Rep. **368**, 549 (2002).
 - [3] A. Parola and L. Reatto, Adv. Phys. **44**, 211 (1995).
 - [4] J. d. Cloizeaux and G. Jannink, *Polymers in Solution: Their Modelling and Structure* (Oxford University Press, 1991).
 - [5] D. Hall, J. Chem. Soc., Faraday Trans. 2 **68**, 668 (1972).
 - [6] R. L. Vink, Soft Matter **5**, 4388 (2009).
 - [7] M. Paoluzzi, C. Maggi, and A. Crisanti, Phys. Rev. Research **2**, 023207 (2020).
 - [8] S. Mertens, I. Jensen, and R. M. Ziff, Phys. Rev. E **96**, 052119 (2017).
 - [9] M. E. Fisher, Phys. Rev. **176**, 257 (1968).
 - [10] H. Hu and Y. Deng, Nucl. Phys. B **898**, 157 (2015).
 - [11] X. S. Chen and V. Dohm, Phys. Rev. E **70**, 056136 (2004).
 - [12] H. Hu, R. M. Ziff, and Y. Deng, Phys. Rev. Lett. **129**, 278002 (2022).
 - [13] V. Dohm, Phys. Rev. E **108**, 044149 (2023).
 - [14] F. Wu, Rev. Mod. Phys. **54**, 235 (1982).
 - [15] G. Grimmett, *The random-cluster model* (Springer, 2006).
 - [16] P. W. Kasteleyn and C. M. Fortuin, J. Phys. Soc. Jpn. **26** (Suppl.), 11 (1969).
 - [17] C. M. Fortuin and P. W. Kasteleyn, Physica **57**, 536 (1972).
 - [18] D. Stauffer and A. Aharony, *Introduction to percolation theory* (Taylor & Francis, 2018).
 - [19] B. Bollobás, G. Grimmett, and S. Janson, Probability Theory and Related Fields **104**, 283 (1996).
 - [20] J. L. Jacobsen, J. Salas, and A. D. Sokal, J. Stat. Phys. **119**, 1153 (2005).
 - [21] M. Łuczak and T. Łuczak, Random Struct. Alg. **28**, 215 (2006).
 - [22] S. Fang, Z. Zhou, and Y. Deng, Phys. Rev. E **103**, 012102 (2021).

- [23] L. Zhang, M. Michel, E. M. Elçi, and Y. Deng, Phys. Rev. Lett. **125**, 200603 (2020).
- [24] Z. Li, Z. Zhou, S. Fang, and Y. Deng, Phys. Rev. E **108**, 024129 (2023).
- [25] H. W. J. Blöte, E. Luijten, and J. R. Heringa, J. Phys. A: Math. Gen. **28**, 6289 (1995).
- [26] Y. Deng and H. W. J. Blöte, Phys. Rev. E **68**, 036125 (2003).
- [27] Z. Zhang, P. Hou, S. Fang, H. Hu, and Y. Deng, Physica A **580**, 126124 (2021).
- [28] R. H. Swendsen and J.-S. Wang, Phys. Rev. Lett. **58**, 86 (1987).
- [29] L. Chayes and J. Machta, Physica **254**, 477 (1998).
- [30] M. Sweeny, Phys. Rev. B **27**, 4445 (1983).
- [31] Z. Peng, E. M. Elçi, Y. Deng, and H. Hu, Phys. Rev. E **108**, 055308 (2023).
- [32] H. W. J. Blöte and Y. Deng, Phys. Rev. E **66**, 066110 (2002).
- [33] Y. Deng and H. W. J. Blöte, Phys. Rev. E **72**, 016126 (2005).
- [34] W. Huang, P. Hou, J. Wang, R. M. Ziff, and Y. Deng, Phys. Rev. E **97**, 022107 (2018).
- [35] N. Metropolis, A. W. Rosenbluth, M. N. Rosenbluth, A. H. Teller, and E. Teller, J. Chem. Phys. **21**, 1087 (1953).
- [36] W. K. Hastings, Biometrika **57**, 97 (1970).
- [37] E. M. Elçi and M. Weigel, Phys. Rev. E **88**, 033303 (2013).
- [38] E. M. Elçi, *Algorithmic and geometric aspects of the random-cluster model*, Ph.D. thesis, Coventry University (2015).
- [39] E. Ben-Naim and P. Krapivsky, Phys. Rev. E **71**, 026129 (2005).
- [40] Y. Deng, W. Zhang, T. M. Garoni, A. D. Sokal, and A. Sportiello, Phys. Rev. E **81**, 020102 (2010).
- [41] H. Saleur and B. Duplantier, Phys. Rev. Lett. **58**, 2325 (1987).
- [42] J. Chayes and L. Chayes, Commun. Math. Phys. **113**, 27 (1987).
- [43] S. Fang, Z. Zhou, and Y. Deng, Chin. Phys. Lett. **39**, 080502 (2022).
- [44] S. Fang, J. Grimm, Z. Zhou, and Y. Deng, Phys. Rev. E **102**, 022125 (2020).
- [45] M. Lu, S. Fang, Z. Zhou, and Y. Deng, Phys. Rev. E **110**, 044140 (2024).
- [46] A. P. Young, Entropy **26**, 509 (2024).
- [47] E. Luijten, *Interaction range, universality and the upper critical dimension* (Delft University Press, 1997).